

High Gain Boost Converter with Charge Pump

B.Vijaykanth¹ | B.Jaya Raju²

¹PG Scholar, Department of EEE, Akula Sree Ramulu Institute of Engineering & Technology, Andhra Pradesh, India.

²Associate Professor, Department of EEE, Akula Sree Ramulu Institute of Engineering & Technology, Andhra Pradesh, India.

To Cite this Article

B.Vijaykanth and B.Jaya Raju, "High Gain Boost Converter with Charge Pump", *International Journal for Modern Trends in Science and Technology*, Vol. 03, Issue 06, June 2017, pp. 92-99.

ABSTRACT

Hybrid DC-DC converter topologies, combining inductor-based switching cells with Switched-Capacitor cells, are gaining an increasing attention in low to medium power applications where the miniaturization and possible integration of the power supply call for a reduction of the magnetic element energy and volume as well as an increase of the switching frequency. The latter, can be attained by reducing the device voltage stress, to keep the associated switching losses to areas onable value. Step-up DC-DC converters are derived combining a basic Buck and Boost cell with a charge pump is studied in this project. Lower DC and AC current levels are obtained in the filter inductor as well as lower device voltage stress compared to an equivalent standard Boost topology. The drawbacks are a floating load connection and possibly higher conduction losses. Simulation results are reported to validate the theoretical analysis and expectations.

Copyright © 2017 International Journal for Modern Trends in Science and Technology
All rights reserved.

I. INTRODUCTION

Solar Photovoltaic (PV) is a key technology option to realize the shift to a decarbonised energy supply and is projected to emerge as an attractive alternative electricity source in the future. Globally, the solar PV grid connected capacity has increased from 9.4 GW in 2007 to 15.7 GW in 2008 and was 67.4 GW at the end of 2012. Nowadays it is necessary to reduce the costs and increase the efficiency to make solar energy to be more useful. As a result, many research works address the development of solar power system in recent years with improved performances. Power electronics is a green technology, converting electrical energy from one form to another, achieving high conversion efficiency of the solar PV-powered system. The efficiency of solar PV powered-system depends mainly on the efficiency of the Maximum Power Point Tracking (MPPT) circuits.

II. PHOTOVOLTAIC ENERGY SYSTEM

The output of solar PV cell is a Direct Current (DC), where the current is determined by the area of the cell and amount of exposed solar irradiation. The voltage of the individual silicon cell is in the order of 0.5V. Thereby, the cell has to be connected in a series to constitute modules with reasonable voltage level. The maximum power is delivered at the operating point, where the magnitudes of PV system and load resistance are equal. This is usually performed by an interfacing DC-DC power converter employing certain MPPT technique and algorithm. The operating point is held at MPP by regulating either the current or voltage of the MPPT converter.

PV systems are usually used in three main fields: 1. Satellite applications, where the solar arrays provide power to satellites, 2. Off-grid applications, where solar arrays are used to power remote loads that are not connected to the electric grid, and 3. On-grid, or grid connected applications, in which

solar arrays are used to supply energy to local loads as well as to the electric grid.

The basic element of the solar PV power conditioning system is the DC-DC converter. If the purpose is to charge a battery or regulate a DC-bus as in space and telecom applications, the system can be implemented by using only the DC-DC converter as depicted

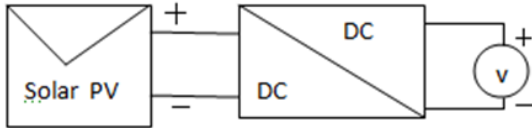


Figure 1.1: Basic element of power conditioning system

III. POWER CONVERTERS IN PV SYSTEM

Photovoltaic system is gaining increased importance as a renewable source because of its advantages such as the absence of fuel cost, little maintenance and no noise and wear due to the absence of moving parts. But there are still two principal barriers to the use of photovoltaic systems: the high installation cost and the low energy conversion efficiency.

A PV panel is a non-linear power source, i.e., its output current and voltage (power) depend on the terminal operating point. The maximum power generated by the PV panel changes with the intensity of the solar radiation and the operating temperature. To increase the ratio of output power/cost of the installation, the PV panel should operate in the maximum output power point.

Modeling of Solar PV Module

A simplified equivalent circuit of a solar cell consists of a diode and a current source which are switched in parallel. The photocurrent generated when the sunlight hits the solar panels can be represented with a current source and the p-n transition area of the solar cell can be represented with a diode. The voltage and current relationship of the simplified solar cell can be derived from Kirchhoff's current law. This simplified equivalent circuit, however, does not give an accurate representation of the electrical process at the solar cell. On real solar cells, voltage losses occur at the boundary and external contacts and leakage currents occur throughout the cell; these losses can be represented with a series resistance R_s and a parallel resistance R_p , respectively. The equivalent circuit of the solar cell showing the series and parallel resistance is shown in Figure 2.4

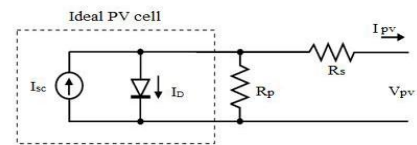


Figure 2.4: Equivalent circuit of a solar PV module

For Figure 2.4, the current equation is given by

$$I_{sc} = I_D + I_{pv} + (V_D / R_p) \quad (2.1)$$

$$V_{pv} = V_D - (I_{pv} * R_s) \quad (2.2)$$

where diode current is $I_D = I_o + (e (V_D / V_t) - 1) I_{sc}$, I_{sc} is the short circuit current, $V_t = N_s K T / q$ is the thermal voltage with N_s cells connected in a series (K is the Boltzmann constant, q is the electron charge and T is the temperature of the PV cells). The short circuit current is directly proportional to the irradiation and slightly proportional to the level of the cell temperature.

Using Equations 2.1 and 2.2, the solar PV module is modeled in MATLAB/Simulink as shown in Figure 2.6 and used to enhance the understanding and predict the I-V and P-V characteristics and to analyze the effect of temperature and irradiation variation. If irradiance increases, the fluctuation of the open-circuit voltage is very small. But the short circuit current has sharp fluctuations with respect to irradiance. However, for a rising operating temperature, the open-circuit voltage is decreased in a non-linear fashion.

The P-V and I-V characteristics are validated in MATLAB software for the L1235-37Wp (Watt peak) solar module. Table 2.1 shows the technical specification of L1235-37Wp solar panel under test which is shown in Figure 2.5. The I-V characteristic is obtained based on experimental results under irradiation = 1000 W/m², temperature = 25°C.

Table 2.1 Specification of a solar PV module under test

| Parameter | Values |
|------------------------------------|------------|
| Open circuit voltage (V_{oc}) | 21V |
| Short circuit current (I_{sc}) | 2.5A |
| Voltage at MPP (V_{max}) | 16.4V |
| Current at MPP (I_{max}) | 2.25A |
| Power rating (P_{max}) | 37W |
| Maximum system voltage | 600V |
| Module efficiency (%) | 10.82% |
| Size (mm) | 645*530*16 |
| Weight (kg) | 4 |

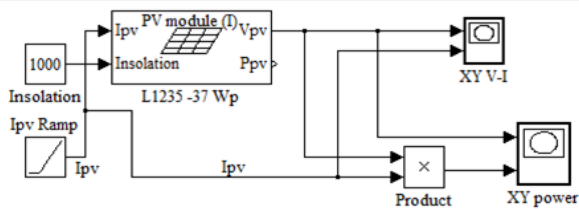


Figure 2.6: MATLAB model for PV module

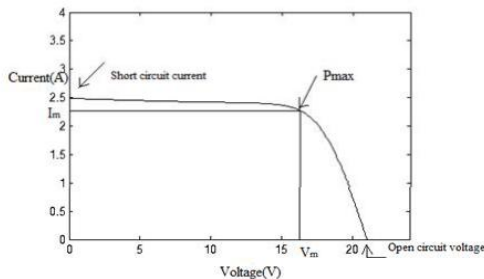


Figure 2.7: I-V Characteristics of solar PV module

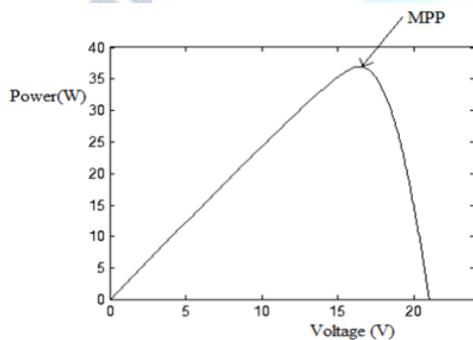


Figure 2.8: P-V Characteristics of solar PV module

IV. MPPT METHODS

The efficiency of energy conversion depends mainly on the efficiency of the PV panels that generate the power. Weather conditions also influence the efficiency, which depends non-linearly on the irradiation level and temperature. When a PV array is directly connected to a load, the system's operating point will be at the intersection of the I-V curves of the PV panel and load. The non-linear variations in the output voltage and current, which depend on solar-radiation levels, operating temperature and load current, can cause a low electrical efficiency. To solve these problems with the utilization of solar arrays for electrical power, the MPP of the PV system (at given conditions) is tracked using offline or online algorithms, where the system operating point is forced towards optimal conditions. The PV array has an optimum operating point called the MPP, which is never constant over time and varies depending on cell temperature and the present irradiation level.

To obtain the maximum power from a PV array, an MPPT is applied. The location of the MPP in the

I-V plane is not known in prior. It can be calculated using a model of the PV array and measurements of irradiance and array temperature, but making such measurements is usually too expensive for this application, and often the required parameters for the PV array model are not known adequately. Thus, the MPPT must continuously search for the MPP of the solar PV module. Many techniques for MPPT of solar PV have been proposed to track maximum power from solar PV module. Some important useful techniques such as hill climbing / Perturb And Observe (PAO), Incremental Conductance (IncCond), fractional open-circuit voltage, fractional short-circuit current, fuzzy logic control, neural network, and Ripple Correlation Control (RCC) are discussed briefly in the following section.

Fuzzy Logic Control

Fuzzy logic control has the advantages of working with imprecise inputs, not needing an accurate mathematical model, and handling nonlinearity. Fuzzy logic control generally consists of three stages: fuzzification, rule base table lookup, and defuzzification. During fuzzification, numerical input variables are converted into linguistic variables based on a membership function.

In this case, five fuzzy levels are used: NB (negative big), NS (negative small), ZE (zero), PS (positive small), and PB (positive big). Seven fuzzy levels are used, probably for more accuracy. The inputs to an MPPT fuzzy logic controller are usually an error E and a change in error E. The user has the flexibility of choosing how to compute E and E.

$$E(n) = \frac{P(n) - P(n-1)}{V(n) - V(n-1)} \quad 2.11$$

$$\Delta E(n) = E(n) - E(n-1) \quad 2.12$$

Once E and E are calculated and converted to the linguistic variables, the fuzzy logic controller output, which is typically a change in duty ratio D of the power converter, can be looked up in a rule base table.

In the defuzzification stage, the fuzzy logic controller output is converted from a linguistic variable to a numerical variable still using a membership function. MPPT fuzzy logic controllers have been shown to perform well under varying atmospheric conditions to track maximum power.

Application-Based Selection of MPPT Algorithm

An MPPT method that has quick response characteristics and is able to make good use of the

electrical power generated under any weather condition is needed to optimize the system management. Many MPPT control methods have been proposed that search for the maximum operating conditions from the output power and voltage characteristics of solar arrays using differential techniques, like the hill-climbing method or fuzzy rules. The main aspects for selection of the MPPT techniques are essentially:

The ease of implementation is an important factor in deciding which MPPT technique to use. Some techniques require analogue circuitry and others digital circuitry, even if that may require the use of software and programming.

The number of sensors required to implement MPPT also affects the selection process. It is easier and more reliable to measure voltage than current. Moreover, current sensors are usually expensive and bulky. It is also uncommon to find sensors that measure irradiance levels, as needed in the linear current controls and the maximum power point current (IMPP) and maximum power point voltage (VMPP) computation methods

The occurrence of multiple local maxima due to partial shading of the PV array can be a real hindrance to the proper functioning of an MPP tracker. Considerable power loss can be incurred if a local maximum is tracked instead of the real MPP;

It is hard to mention the monetary costs of every single MPPT technique unless it is built and implemented. A good cost comparison can be made by knowing whether the technique is analogue or digital, whether it requires software and programming, and the number of sensors. Analogue implementation is generally cheaper than digital, which normally involves a microcontroller that needs to be programmed;

Different MPPT techniques will suit different applications. For example, in space satellites and orbital stations that involve a large amount of money, the costs and complexity of the MPP tracker are not as important as its performance and reliability. The tracker should be able to continuously track the true MPP in minimum amount of time and should not require periodic tuning. In this case, hill climbing/PAO, IncCond, and RCC are appropriate. Solar vehicles would mostly require fast convergence to the MPP. Fuzzy logic control, neural network, and RCC are good options in this case. Since the load in solar vehicles consists mainly of batteries, load current or voltage maximization should also be considered. The goal, when using PV arrays in residential areas, is to minimize the payback time and to do so, it is

essential to constantly and quickly track the MPP. Since partial shading (from trees and other buildings) can be an issue, the MPPT should be capable of bypassing multiple local maxima. Therefore, the two-stage IncCond and the current sweep methods are suitable. Since a residential system might also include an inverter, the open circuit voltage MPPT can also be used. PV systems used for street lighting only consist of charging up batteries during the day. They do not necessarily need tight constraints; easy and cheap implementation might be more important, making fractional VOC or ISC viable.

The method considered in this research work is a PAO method. This method is widely diffused because of its low-cost and ease of implementation. When atmospheric conditions are constant or change slowly, the PAO method oscillates close to MPP. However, when these change rapidly, this method fails to track MPP and gives rise to a waste of part of the available energy.

The main limitation of this kind of algorithm is connected with the opposite exigencies required by the fast dynamic response and the steady-state stability. Indeed, to improve the dynamic performance it is necessary to use a large perturbation value, whereas a smaller value is necessary to ensure good stability. During cloudy days, the solar irradiation can vary many times and quickly. Because of this, so as not to lose great quantities of energy, it is necessary to achieve a good dynamic response for the system. The basic principle of the algorithm proposed is to adapt the perturbation amplitude to the actual operating conditions. In particular, far from the MPP, large perturbation amplitudes are chosen, whereas small ones are used in proximity to the maximum. It is therefore necessary to have knowledge of the maximum position. However, a perfect knowledge is not required because working at the real maximum is ensured by the PAO technique. An adaptive PAO method is discussed and implemented in this research. It has faster dynamics and improved stability compared to the traditional PAO.

SEPIC Converter

In a Single Ended Primary Inductor Converter (SEPIC) converter, the output voltage can be higher or lower than the input voltage. Unlike the buck-boost, the output is not inverted. The SEPIC converter shown in Figure 3.5 uses two inductors, L1 and L2. The capacitor C1 isolates the input from the output and provides protection

against a shorted load when the switch S is turned on. The first inductor, L1, is charged from the input voltage source during this time. The second inductor takes energy from the first capacitor, and the output capacitor is left to provide the load current. The fact is that both L1 and L2 are disconnected from the load when the switch is on. When the power switch is turned off, the first inductor charges the capacitor C1 and also provides current to the load. The second inductor is also connected to the load during this time. The output capacitor sees a pulse of current during the off time, making it inherently noisier than a buck converter.

The relation between input and output currents and voltage is given by

$$\frac{V_O}{V_{IN}} = \frac{d}{(1-d)}$$

$$\frac{I_{IN}}{I_o} = \frac{d}{(1-d)}$$

The input current is non-pulsating. In SEPIC converter, link- capacitor (C1) voltage must follow the input voltage, and this means that the capacitor size can be smaller. So the SEPIC converter is suitable in MPP tracking process.

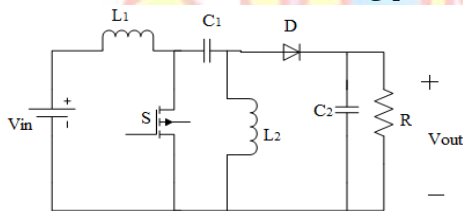


Figure 3.5: SEPIC converter

Cuk Converter

The basic circuit configuration used in Cuk converter is shown in Figure 3.6. Cuk converter has two modes of operation. The first mode of operation is when the switch (MOSFET) is closed (ON) and it is conducting as a short circuit as shown in Figure 3.7. In this mode, the current through inductor L1 rises. At the same time, the voltage of capacitor C1 reverse biases the diode D and turns it off. The capacitor (C1) releases its stored energy to the load. The second operating mode is when the switch (S) is open (OFF), diode (D) is forward biased and conducting energy to the output as shown in Figure 3.8. Capacitor C1 is charging from input supply and the energy stored in the inductor L2 is transferred to the load. The diode D and switch (S) provide a synchronous switching action given by

$$\frac{V_O}{V_{IN}} = - \frac{d}{(1-d)} \quad \frac{I_{IN}}{I_o} = - \frac{d}{(1-d)}$$

The input resistance of Cuk converter R_i during the continuous conduction mode is given by

$$R_i(\text{CCM}) \in [0, \infty] \quad R_i(\text{CCM}) = \frac{2 L_{eq} * f_s}{d^2} \quad \text{where}$$

$$L_{eq} = L1 // L2 \quad \text{and } f_s \text{ - switching frequency}$$

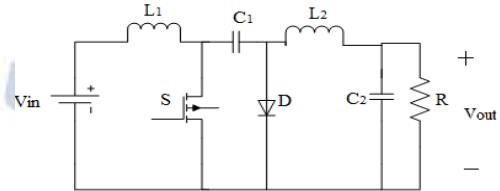


Figure 3.6: Cuk converter

The input resistance R_i during the discontinuous conduction mode is given by

$$R_i(\text{DCM}) = \frac{KR}{d^2}$$

Therefore, the Cuk converter is capable of sweeping the whole I-V curve of a solar PV module in CCM from open circuit voltage (V_{oc}) to short circuit current (I_{sc}) condition

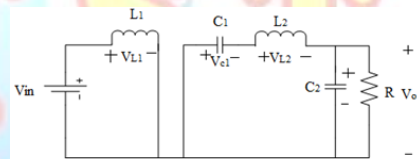


Figure 3.7: Mode 1: Switch S is ON

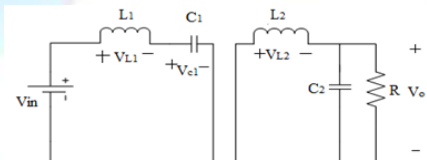


Figure 3.8: Mode 2: switch S is OFF

Due to the input and output inductor in Cuk converter, the input current is non-pulsating. Therefore, the sweep of the I-V curve is carried out in a more reliable and less noisy way. So Cuk converter is more suitable in MPP tracking circuits. The Cuk converter is preferred in power conditioning process of solar PV system since Cuk converter works based on the energy transfer of the capacitor and hence less EMI.

V. PROPOSED SRM DRIVE CONVERTER

A. Converter Topology

Fig. (4) shows the per phase structure of the proposed SRM drive topology. The converter operation is simple with a minimum number of switches while performing phase

current commutation quickly. Regarding the number of switches used, the converter is similar to the R-dump converter, and its functions like the C-dump converter since the phase inductance energy is recovered. In fact, in addition to its simple structure, this converter has higher efficiency than the R-dump converter and a simpler structure and higher phase current commutation speed than the C-dump converter.

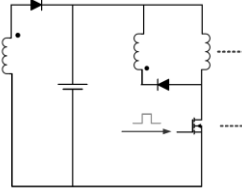
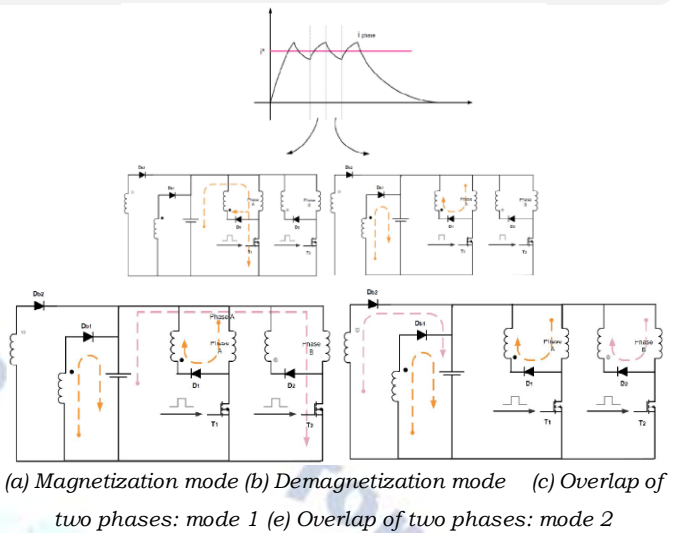


Fig. 4. Proposed SRM per phase converter

Fig. (5) shows the operating modes of this converter for 2 phase SRM. As shown in Fig. (5-a), in the magnetization mode, the switch T1 turns on in order to magnetize phase 'a'. As T1 turns on, the energy is transferred from the source to phase winding and the current in phase inductance increases. Also, in this mode if the magnetizing inductance of coupled inductors is not reset yet, diode D1 would conduct the magnetizing inductance current of the coupled inductors and the input voltage would reset this inductor. When the magnetizing inductance of coupled inductors is reset, Diode D1 turns off. The reset of coupled inductors magnetizing inductance is similar for other phases.

When the phase current reaches the reference, T1 is turned off and demagnetization starts. This mode is shown in Fig. (5-b). Since the voltage across phase winding is reversed, diode D1 turns on in this mode. When D1 turns on, D1 turns on and a negative voltage is placed across the phase winding in proportion to the coupling ratio which accelerates phase current commutation. Fig.(5-c) and Fig. (5-d) show two overlapping modes of stator phase currents. In the first mode, the phase inductance 'a' is being demagnetized and phase 'b' is being magnetized. In the second mode, both 'a' and 'b' phases are being demagnetized. As it can be observed, this converter has the ability to separately control phase currents. Also, it is important to notice that the snubber circuit of each switch will absorb the voltage spikes across the switches that otherwise would occur due to leakage inductance of coupled inductors.



(a) Magnetization mode (b) Demagnetization mode (c) Overlap of two phases: mode 1 (d) Overlap of two phases: mode 2

B. Design considerations

For designing this converter, the coupled inductors ratio has to be determined considering the performing speed of the drive. As shown in Fig. (1), if the phase current does not reach zero fast enough during the commutation, the phase current continues to exist in the negative torque production area and the phase torque becomes negative. This negative torque will cause large ripples in the torque generated by the motor. This is especially important at higher speeds, because higher speed requires faster commutation. So, each SRM drive can function to an extent of speed with regard to its converter's structure. The maximum SRM drive speed depends on the type of converter used and is illustrated by the following equation $T_f = \tau_a \ln \left[1 + \frac{R_s I_p}{V_c} \right]$ (1)

where T_f is the time needed for the current to reach from reference value to zero, τ_a is the electrical time constant of machine phases, R_s is the resistance of each phase winding, V_c is the reverse voltage applied to the phase inductance during commutation. The electrical time constant equation of the machine is as follows

$$\tau_a = \frac{L_a}{R_s} \quad (2)$$

As shown in Fig. (1), the phase inductance at the current commutation area equals to aligned inductance, thus L and τ would take an "a" subscript. Current drop angle at speed ω is shown as θ_f in Fig. (1) and is calculated as follows. $\theta_f = \omega_m T_f = [\omega_m \tau_a] \ln \left[1 + \frac{R_s I_p}{V_c} \right]$ (3)

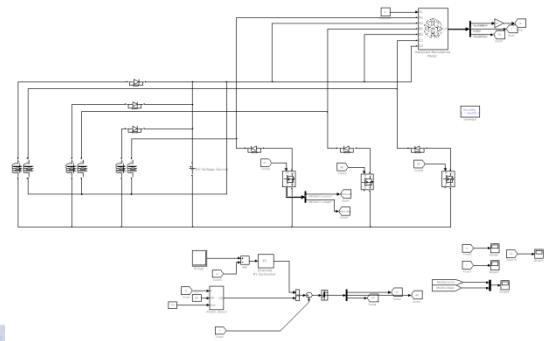
As it can be observed from (3), when speed increases, θ_f becomes larger resulting in a larger negative torque and, consequently, more torque ripples. Therefore, it is needed to look for a way to reduce θ_f at higher speeds. As it can be observed

from (3), commutation can be carried out faster by increasing V_c . In the proposed converter, the reverse voltage across the phase winding can be increased for faster commutation purposes by increasing the coupled inductors L_1 and L_2 turns ratio. Also it is important to notice that V_c is constant in most of the converters introduced so far. But, in this converter, V_c can be designed by changing the coupled inductors turns ratio considering the maximum SRM drive functioning speed.

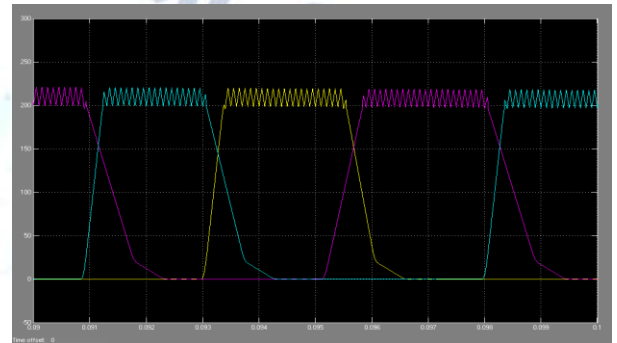
VI. SIMULATION RESULTS

In this section, the simulation results of SRM drive using the proposed converter is compared to the results of a SRM drive that uses a regular asymmetric converter. The schematic of this converter is shown in Fig. 6.

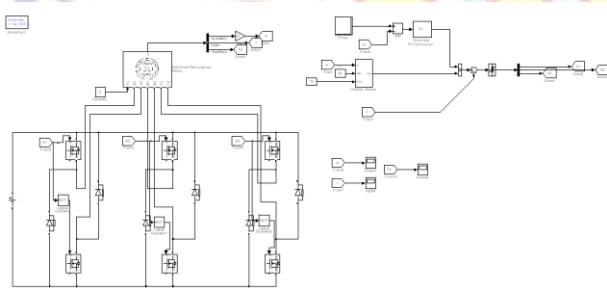
For simulation purposes coupling ratio is selected 2.3. Figure (7) shows the SRM phase currents that are driven by a regular asymmetric converter at 1500 rpm. Figure (8) shows the phase currents of the same motor at 4000 rpm.



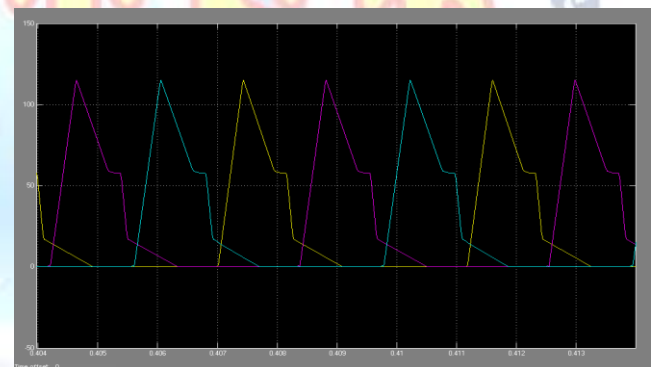
Simulink diagram of Proposed converter



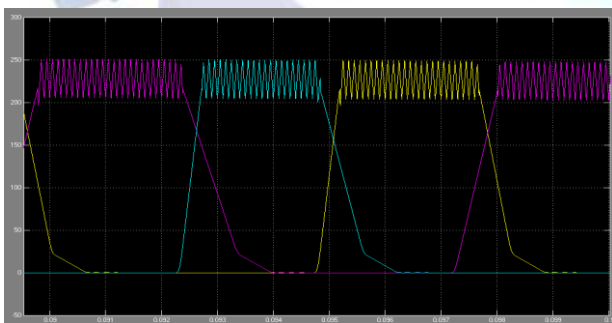
Phase current waveforms of SRM driven by proposed converter at 1500 rpm.



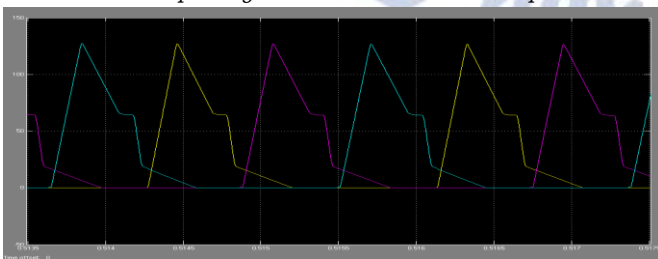
Simulink diagram of Asymmetric converter



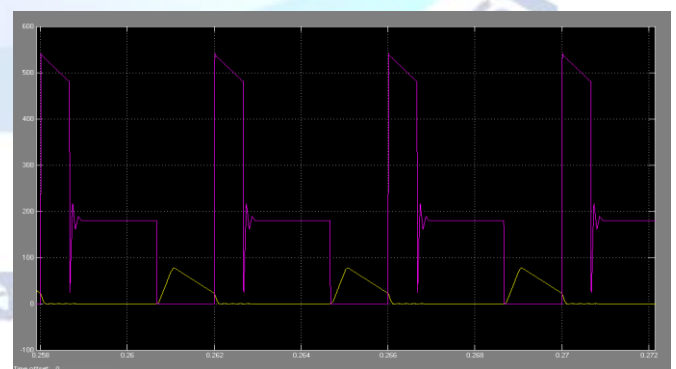
Phase current waveforms of SRM driven by proposed converter at 4000 rpm.



Phase current waveforms of SRM driven by asymmetric converter at 1500 rpm asymmetric converter at 4000 rpm.



Phase current waveforms of SRM driven by asymmetric converter at 4000 rpm.



Voltage and current waveforms of one switch

VII. CONCLUSIONS

The design of a low cost PV powered SRM employed irrigation pump using a boost converter has been suggested and appropriateness of it has

been demonstrated through examining its various responses in MATLAB/Simulink platform. A simple and efficient method for speed control of SR motor has been achieved, which provides the privilege for reduction of current sensors on the motor side. The PWM switching of a mid-point converter has been utilized which requires small rating split capacitors. The controlled starting of SR motor has been achieved using the perturbation size adjustment in the MPPT controller. The occasional self-start failure of 4-phase SR motor has been also acknowledged in proposed system and it has efficiently eliminated by implementing appropriate commutation angle dependent control. The overall behavior of proposed system even under rapidly changing environmental conditions concludes its suitability for PV based irrigation system

REFERENCES

- [1] K. Hyung, H. Shin, J. I. Ha and A. Yoo, "Efficiency control of multistring PV system considering switching losses analysis," In Proc. of IEEE Applied Power Electronics Conference and Exposition – APEC2014, Fort Worth, TX, 2014, pp. 3143-3149.
- [2] J. D. Bastidas-Rodriguez, E. Franco, G. Petrone, C. A. Ramos-Paja and G. Spagnuolo, "Maximum power point tracking architectures for photovoltaic systems in mismatching conditions: a review," IET Power Electronics, vol. 7, no. 6, pp. 1396-1413, June 2014.
- [3] X. Xiao, X. Huang and Q. Kang, "A Hill-Climbing-Method-Based Maximum-Power-Point-Tracking Strategy for Direct-Drive Wave Energy Converters," IEEE Transactions on Industrial Electronics, vol. 63, no. 1, pp. 257-267, Jan. 2016.
- [4] M. H. Uddin, M. A. Baig and M. Ali, "Comparision of 'perturb & observe' and 'incremental conductance', maximum power point tracking algorithms on real environmental conditions," in Proc. International Conference on Computing, Electronic and Electrical Engineering (ICE Cube), Quetta, Pakistan, 2016, pp. 313-317.
- [5] R. J. K. Prasana, S. Ramprasath and N. Vijayarathi, "Design and analysis of hybrid DC-DC boost converter in continuous conduction mode," in Proc. International Conference on Circuit, Power and Computing Technologies (ICCPCT), Nagercoil, 2016, pp. 1-5.
- [6] N. Chandrasekaran and K. Thyagarajah, "Modeling and performance study of single phase induction motor in PV fed pumping system using MATLAB," Int. J. Electr. Eng., vol. 5, no. 3, pp. 305-316, 2012.
- [7] R. Antonello, M. Carraro, A. Costabeber, F. Tinazzi and M. Zigliotto, "Energy-efficient autonomous solar water-pumping system for permanent magnet synchronous motors," IEEE Transactions on Industrial Electronics (Early Access).
- [8] H. Hembach, S.A. Evans and D. Gerling, "Systematic comparison of BLDC motors for small automotive water pump applications," in Proc. of 18th International Conference on Electrical Machines, ICEM2008, 6-9 Sept. 2008, pp.1-5.
- [9] B. Singh and R. Kumar, "Simple brushless DC motor drive for solar photovoltaic array fed water pumping system," IET Power Electronics, vol. 9, no. 7, pp. 1487-1495, 6 8 2016.
- [10] J. H. R. Enslin and D. B. Snyman, "Combined low-cost, high-efficient inverter, peak power tracker and regulator for PV applications," IEEE Transactions on Power Electronics, vol. 6, no. 1, pp. 73-82, Jan 1991